ChemComm

Chemical Communications

outside

twist

7 nm

50 nm

150 nm

inside

150 nm

growth

50 nm

core

15 nm

fast - MAS NMR

ROYAL SOCIETY
OF CHEMISTRY
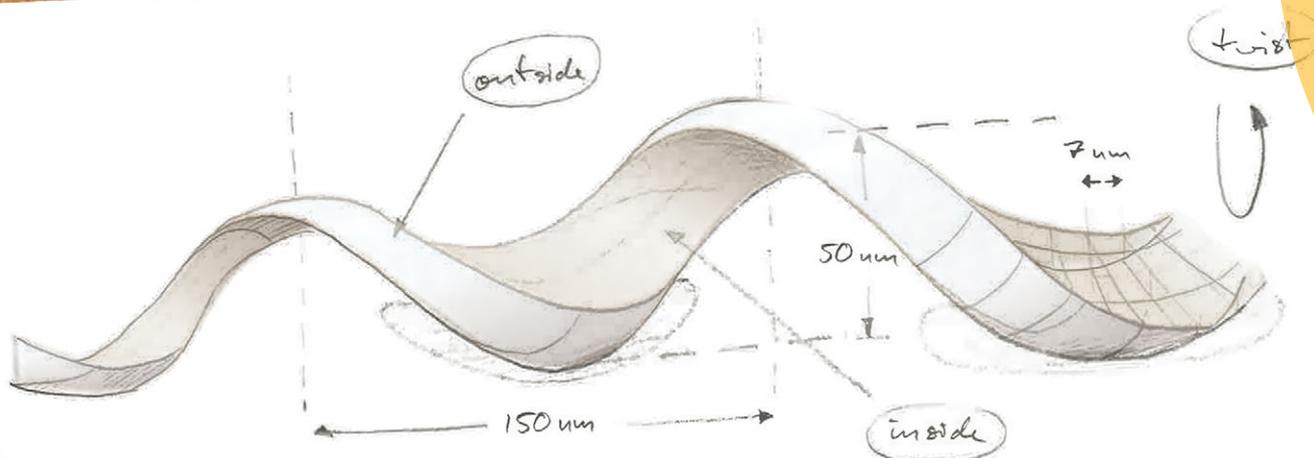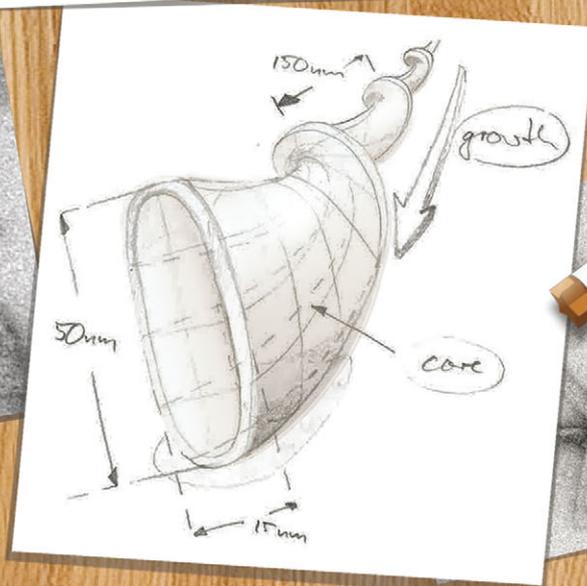
COMMUNICATION
Rasmus Linser *et al.*
Backbone assignment for minimal protein amounts of low structural
homogeneity in the absence of deuteration

175 YEARS

Backbone assignment for minimal protein amounts of low structural homogeneity in the absence of deuteration†

ShengQi Xiang,[a] Jacek Biernat,[bc] Eckhard Mandelkow,[bc] Stefan Becker[a] and Rasmus Linser*[a]

NMR characterization of many proteins is limited by low expression, hurdles for deuteration, and poor sample homogeneity. We introduce a set of high-dimensionality proton-detected experiments developed for unambiguous resonance assignments of such proteins, which we could successfully apply to a 1 mg amount of non-deuterated Tau paired helical filaments.

Since the development of proton-detection technology,[1–3] the sensitivity of solid-state NMR spectroscopy can be increased manifold using protons as a detection nucleus rather than ^{13}C.[4,5] In addition, proton-detected NMR bears the possibility of using protons as an additional source of information useful for resonance assignments[6–8] and structure calculation[9–11] and also as a reporter on protein dynamics[12–15] and interactions.[16–18] This technology was first developed using perdeuterated samples partially ^{1}H-back exchanged at amide sites. Intuitively, with increasingly fast Magic-Angle-Spinning (MAS) speeds due to advances in hardware development, the degree of back-protonation could be increased.[11,20–22] This now enables usage of fully protonated proteins with an unprecedented sensitivity per amount of sample. For many proteins, usage of minimal amounts of fully protonated samples is the only option available. Thus, these possibilities have the potential to circumvent a major bottleneck in sample preparation.

NMR studies of proteins usually build on sequential assignments obtained from intra- and interresidual backbone chemical shifts. In pioneering work, ^{1}H-detection-based backbone assignments of fully protonated proteins have already been achieved at 40 kHz MAS.[23,24] It was then shown for 60 kHz MAS that backbone assignment experiments similar to those previously demonstrated

for ^{1}H^{N} back-exchanged samples[4,6,25] could also be applied to fully protonated proteins.[26] A new generation of probes can now provide spinning speeds of more than 100 kHz. This has been applied to amide-back-exchanged protein preparations[22,27] and further increases the viability of fully protonated samples.[28]

Previously, ^{13}C-shift-based assignment strategies using proton-detected experiments like 3D hCANH, hcaCBcaNH, hCOcaNH and many more have been shown.[6,25,29] Also, proton-detected 4D sequences like hCACOCaNH have been demonstrated for partially proton back-exchanged proteins.[30] Recently, amide-to-amide correlations using sequential magnetization transfers were presented for the first time in the solid state on ^{1}H^{N} back-exchanged samples.[31,32]

Here we specifically tackle such protein preparations that deviate from the most ideal situation (deuterated, microcrystalline proteins), *i.e.* that suffer from coherent effects due to proton dipolar couplings and poor sample homogeneity. For this, we (i) turn to higher-dimensionality, complementary assignment strategies. In addition, we (ii) tailor the ^{13}C-based sequences such that they contain no out-and-back elements, which are not necessary because of the ubiquitous presence of protons. (iii) We employ transfer schemes that are as independent of transverse relaxation times and coherent effects as possible: As such, we only employ purely dipolar-coupling-based methodology for the fully protonated samples to correlate amide chemical shifts with backbone and side chain carbon shifts, with inter-residual amide nitrogen shifts, and with aliphatic protons. In addition to backbone heteronuclei, these aliphatic proton shifts are well accessible (see details below). We used the fully protonated SH3 domain of α-spectrin for pulse scheme development and successively applied these experiments to Tau paired helical filaments (PHFs), which occur in the course of Alzheimer's disease[33] and have as yet posed significant hurdles for solid-state NMR due to sample heterogeneity.

Fig. 1 shows the pulse programs developed in this study. All experiments are in a straight-through manner because of the omnipresent protons in the samples. In the two 4D experiments (Fig. 1A), (H)COCANH and (H)CACONH, the C^{α} and C′

[a] *Max-Planck Institute for Biophysical Chemistry, Department NMR-Based Structural Biology, Am Fassberg 11, 37077 Göttingen, Germany.*
E-mail: rali@nmr.mpibpc.mpg.de
[b] *DZNE, German Center for Neurodegenerative Diseases, Ludwig-Erhard-Allee 2, 53175 Bonn, Germany*
[c] *CAESAR Research Center, Ludwig-Erhard-Allee 2, 53175 Bonn, Germany*
† Electronic supplementary information (ESI) available: Comprehensive experimental details. See DOI: 10.1039/c5cc09160h
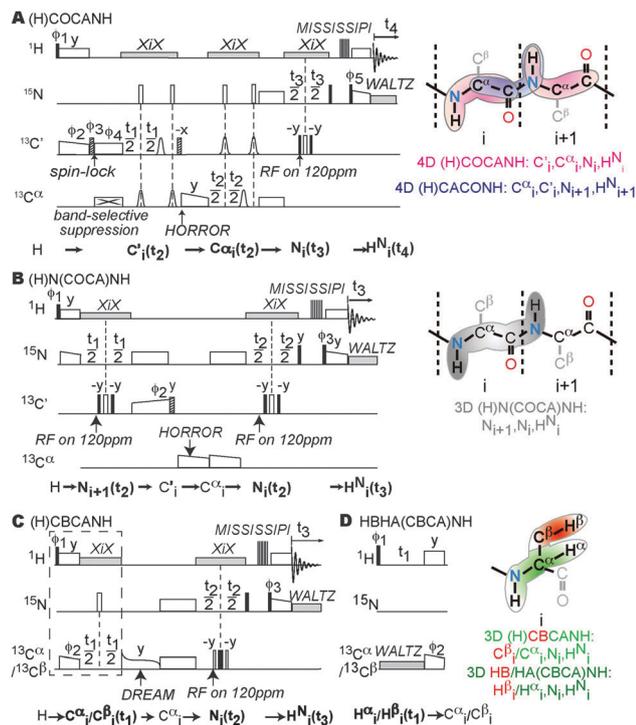
Fig. 1 Pulse programs and correlations. (A) 4D (H)COCANH pulse program to obtain intra-residual H_i^N, N_i, C_i^α, C_i' correlations. The complementary (H)CACONH experiment is obtained by swapping the C' and C$^\alpha$ channels. (B) (H)N(COCA)NH pulse program to obtain H_i^N, N_i and N_{i+1}. (C) Pulse program of (H)CBCANH. Replacing the box by (D) results in the HBHA(CBCA)NH experiment. Open, filled, and striped bars represent 90°, 180°, and trim pulses, respectively. Bell shapes indicate selective 180″ pulses on C' and C$^\alpha$. The rectangles and trapezoids are spin-lock pulses in cross-polarization. The train of proton pulses for water saturation follows the MISSISSIPI.[19] The magnetization transfer pathways are shown below each pulse program. The schematic representations of the correlations obtained from each pulse program are listed next to them. Details about the pulse program can be found in the ESI.†
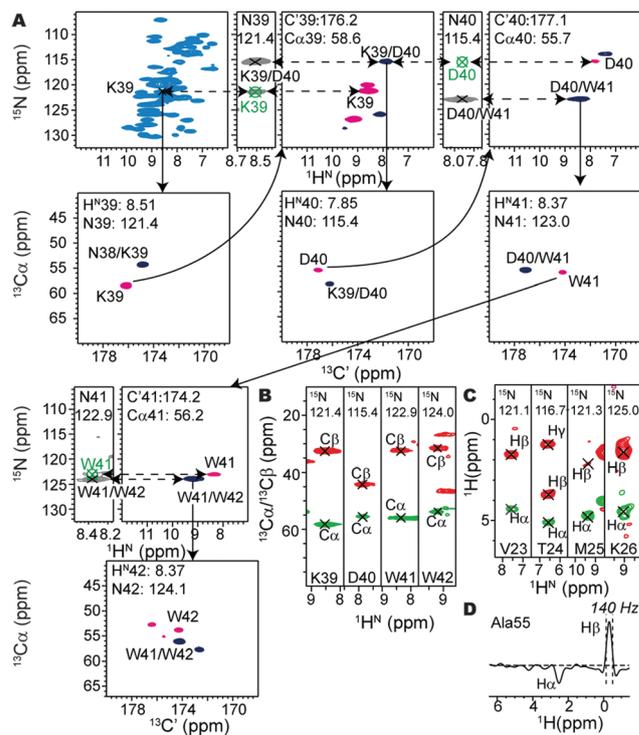

Fig. 2 Assignment of a fully protonated SH3 sample at 55.5 kHz. (A) Backbone walk from a combination of two 4D experiments, (H)CACONH (blue) and (H)COCANH (magenta), and a 3D (H)N(COCA)NH (gray). The 2D spectrum in the upper left corner is the 2D H^N–N correlation spectrum, the rest are 2D planes extracted from 4D spectra, depicted as H^N/N planes (1st and 3rd row) and C$^\alpha$/C' planes. The chemical shifts of the non-paper-plane dimensions are shown in the upper-left corner of each 2D or strip. Next to every H^N/N plane is an (H)N(COCA)NH strip from the shifts of the same amide group of the detected proton. Green and black crosses denote the diagonal and inter-residual positions, respectively. Arrows correspond to the workflow during the walk along the backbone. Dashed double-headed arrows connect pairs of peaks with the same chemical shifts in the N dimension between strips and planes. (B) Strips from HBHA(CBCA)NH for the residues from K39 to W42. (C) Strips from HBHA(CBCA)NH corresponding to the sequence from V23 to D29. Negative and positive peaks in (B) and (C) are shown in green and red, respectively. (D) 1D trace of HBHA(CBCA)NH of Ala55 showing the homogeneous linebroadening of the aliphatic proton signals.

are correlated either with the inter- or the intra-residual amide group, respectively. Two-dimensional matching of chemical shifts (i.e. nuclear pairs C$^\alpha$/C' or N/H^N) enables unambiguous identification of sequential connections while progressing along the protein backbone (see Fig. 2 and details below). In addition to ^{13}C backbone chemical shifts, we and others have recently suggested direct amide-to-amide correlations for backbone assignments in deuterated proteins,[31,32] for which a pulse sequence is depicted in Fig. 1B. Employing the above-mentioned strategies, such correlations turn out even more desirable when deuteration is absent. Combined with the two 4D experiments mentioned above, remaining ambiguities in sequential searching can be minimized since N, C$^\alpha$, and C' shifts are employed at the same time. A potential drawback of using dipolar homonuclear transfers is residual magnetization on the source nucleus, which can be alleviated by a band-selective suppressing module to remove unwanted signals.[34] The efficacy of this module is demonstrated in ESI,† Fig. S1.

For assigning the backbone, sequential-connectivity information only is usually not enough. Residue type information is also needed, which usually requires at least side chain C$^\beta$ chemical shifts. C$^\alpha$/C$^\beta$ chemical shifts can be obtained from an experiment in which C$^\alpha$/C$^\beta$ are correlated to the intra-residual amide group. This sequence is shown in Fig. 1C. A bonus of fully protonated samples is the availability of aliphatic proton chemical-shift information. Their characterization will be of increasing importance for both, structural features of solid-state NMR as well as interactions with the solvent, lipids, small molecules, and other proteins. The proton shift can be obtained in a straightforward way by an HAHB(CBCA)NH experiment (Fig. 1D) which we modified from the (H)CBCANH by moving the first evolution time from C$^\alpha$/C$^\beta$ to H$^\alpha$/H$^\beta$. Hence the H$^\alpha$ and H$^\beta$, instead of C$^\alpha$ and C$^\beta$, will be correlated with the backbone amide groups.

We first tested these pulse programs for ^{13}C,^{15}N SH3 domain of α-spectrin at 55.5 kHz MAS on an 800 MHz Bruker AVANCE III spectrometer. Comprehensive experimental details as well as a

sensitivity comparison (Fig. S2) can be found in the ESI.†
Backbone assignment from residue 39 to 42 is demonstrated
in Fig. 2. The assignment strategy is similar as previously
reported for a dipolar HNCACO out-and-back experiment:[30]
the amide N and proton chemical shifts of K39 obtained from
a 2D (H)NH correlation spectrum (the upper left panel in
Fig. 2A) can be used to obtain correlated carbon shifts from
C^α–C' 2D planes in 4D space. In the 4D, the blue peaks
represent the (H)CACONH spectrum and reveal the inter-
residue correlation to the previous residue. The magenta peaks
show the (H)COCANH spectrum providing the intra-residual
correlations. Intraresidual K39 (H)COCANH carbon shifts navi-
gate to the NH plane from which the next residue can be found:
In this plane, in addition to the magenta intraresidual peak
(K39), the blue (H)CACONH peak shows up with amide shifts of
D40. With these shifts, navigation to the next C^α–C' plane is
enabled, where the newly appearing magenta peak now also
provides D40's carbon shifts, and so on. The well-separated peaks
in 4D space and low ambiguities resulting from simultaneous
matching of two chemical shift values make this assignment
strategy highly effective.

3D strips from (H)N(COCA)NH at the amide shifts of each
residue i are shown next to the 2D HN planes, in which inter-
residual correlations marked with a black cross provide the
amide nitrogen shift of the next residue. The redundant weak
autocorrelation peak marked in green is sometimes present
but not necessarily needed. This amide-to-amide correlation
enables cross-validation for identification of connectivities, as
shown by the dashed double-headed arrows in Fig. 2A.

With the sequential connections established, the C^α and C^β
shifts obtained from the (H)CBCANH are used to identify the
residue types, thus enabling mapping of obtained fragments
to the primary sequence (Fig. 2B). Once backbone assign-
ment is achieved, H^α/H^β shifts can be read out from the
HBHA(CBCA)NH experiment. The H^α/H^β strips from V23 to
K26 are shown in Fig. 2C. Due to the use of a DREAM transfer,
the C^α/H^α and C^β/H^β peaks have opposite signs. Recording
proton-detected amide-to-aliphatic-proton correlations in non-
deuterated SH3 at 55 kHz, we obtain proton line widths on the
order of 250 Hz to 300 Hz for aliphatic protons. Methyl protons
yield line widths on the order of 150 Hz (Fig. 2D).

Having established a robust assignment strategy for non-
deuterated proteins with little spectral dispersion, we were in
the position to apply this to fibrils of the repeat domain of Tau
protein (construct K19[35] C322A). Tau is a natively unfolded
neuronal protein involved in the stabilization of microtubules.
In pathological conditions of Alzheimer's disease and other
tauopathies, the repeat domain of tau causes aggregation into
fibers termed "paired helical filaments" (PHFs).[33] This protein
has not been expressed in deuterated media to date and the
preparations of PHFs give rise to heterogeneity, which has
made standard experimental strategies very challenging and
costly. Accordingly, despite work by different groups,[36,37] no
Tau PHF structure has been obtained yet.

In Fig. 3 we show a successful excerpt of the assignments
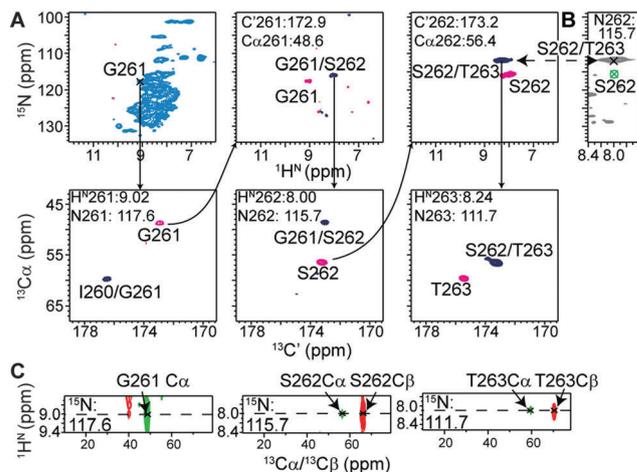obtained for a 1 mg sample of the K19 variant C322A. In this

Fig. 3 Backbone and side chain assignments applied to Tau K19 paired
helical filaments. (A) Sequential backbone walk starting from G261 to T263
based on 4D (H)COCANH (in magenta) and 4D (H)CACONH (in blue). The
intra-residual correlation peaks are labeled by residue number, while
the inter-residual peak labels denote the two residues they connect. (B)
The (H)N(COCA)NH strip at the position of the amide group of S262
confirms the N shift value of (next residue) T263. This value matches the
connections found in the 4D experiments, as indicated by dash arrow. (C)
Corresponding strips from an (H)CBCANH experiment, providing informa-
tion about residue type. Positive peaks of C^β are shown in red and negative
peaks of C^α in green.

sample, homogeneous and heterogeneous linebroadening
cause proton line widths between 250 and 500 Hz at 55.5 kHz
MAS (see Fig. S4, ESI†). The backbone walk based on two 4D
experiments ((H)N(COCA)NH and (H)N(CACO)NH) is shown in
panel A. The amide-to-amide experiment in its 3D (H)N(COCA)NH
fashion (panel B) was then used to cross-validate the connections
obtained: here, the N chemical shifts of T263 from 4D experi-
ments and amide-to-amide experiments are identical and the
residues can be connected with high confidence despite the large
linebroadening of the preparation. Finally, the strips from the
(H)CBCANH experiment, correlating the C^β shift with the amide
group chemical shifts of each residue, are displayed in panel C.
Based on the C^β/C^α chemical shifts, it is clear that this fragment
represents the sequence "GST". In contrast to most other residues
assigned, this fragment is unambiguously located in a stretch that
was not reported in previous work on this construct.[37] A second
representative backbone walk and all assignments obtained are
shown in Fig. S3–S5 (ESI†).

Considering the Double Quantum (DQ) condition employed
in the transfer steps, the pulse programs presented here should
be well suitable for the fastest spinning speeds (>100 kHz)
reached currently in a few groups or more widely in the
near future. Assuming an increasingly effective averaging of
proton dipolar couplings at faster MAS speeds, J-coupling-
based approaches could again become an alternative to the
dipolar-coupling-based cross polarization even in the absence
of deuteration.[27] In this case, the transfer steps in the current
pulse programs can be adapted to actual conditions, while the
other components of the assignment strategy would remain
appropriate.

In conclusion, we have presented high-dimensionality proton-detected experiments to obtain sequential resonance assignments on minimal, non-deuterated sample amounts despite short coherence lifetimes and sample heterogeneity. These involve backbone spins and aliphatic proton shifts in fully protonated proteins at fast MAS. As demonstrated in the case of the heterogeneous Tau paired helical filaments, this approach will facilitate the study of such challenging systems which provide hurdles in terms of sample volume limitations, incompatibility with deuteration, and spectral overlap due to sample heterogeneity or the number of resonances.

References

1 E. K. Paulson, C. R. Morcombe, V. Gaponenko, B. Dancheck, R. A. Byrd and K. W. Zilm, *J. Am. Chem. Soc.*, 2003, **125**, 14222–14223.
2 V. Chevelkov, K. Rehbein, A. Diel and B. Reif, *Angew. Chem., Int. Ed.*, 2006, **45**, 3878–3881.
3 A. E. McDermott, F. J. Creuzet, A. C. Kolbert and R. G. Griffin, *J. Magn. Reson.*, 1992, **98**, 408–413.
4 M. J. Knight, A. L. Webber, A. J. Pell, P. Guerry, E. Barbet-Massin, I. Bertini, I. C. Felli, L. Gonnelli, R. Pierattelli, L. Emsley, A. Lesage, T. Herrmann and G. Pintacuda, *Angew. Chem., Int. Ed.*, 2011, **50**, 11697–11701.
5 A. Tregubov, R. Linser, K. Q. Vuong, A. Rawal, J. Gehman and B. Messerle, *Inorg. Chem.*, 2014, **53**, 7146–7153.
6 R. Linser, M. Dasari, M. Hiller, V. Higman, U. Fink, J.-M. Lopez del Amo, S. Markovic, L. Handel, B. Kessler, P. Schmieder, D. Oesterhelt, H. Oschkinat and B. Reif, *Angew. Chem., Int. Ed.*, 2011, **50**, 4508–4512.
7 R. Linser, U. Fink and B. Reif, *J. Am. Chem. Soc.*, 2010, **132**, 8891–8893.
8 E. Barbet-Massin, A. J. Pell, J. S. Retel, L. B. Andreas, K. Jaudzems, W. T. Franks, A. J. Nieuwkoop, M. Hiller, V. Higman, P. Guerry, A. Bertarello, M. J. Knight, M. Felletti, T. Le Marchand, S. Kotelovica, I. Akopjana, K. Tars, M. Stoppini, V. Bellotti, M. Bolognesi, S. Ricagno, J. Chou, R. G. Griffin, H. Oschkinat, A. Lesage, L. Emsley, T. Herrmann and G. Pintacuda, *J. Am. Chem. Soc.*, 2014, **136**, 12489–12497.
9 R. Linser, B. Bardiaux, V. Higman, U. Fink and B. Reif, *J. Am. Chem. Soc.*, 2011, **133**, 5905–5912.
10 M. Huber, S. Hiller, P. Schanda, M. Ernst, A. Böckmann, R. Verel and B. H. Meier, *ChemPhysChem*, 2011, **12**, 915–918.
11 M. J. Knight, A. J. Pell, I. Bertini, I. C. Felli, L. Gonnelli, R. Pierattelli, T. Herrmann, L. Emsley and G. Pintacuda, *Proc. Natl. Acad. Sci. U. S. A.*, 2012, **109**, 11095–11100.
12 V. Chevelkov, Y. Xue, R. Linser, N. Skrynnikov and B. Reif, *J. Am. Chem. Soc.*, 2010, **132**, 5015–5017.
13 V. Chevelkov, U. Fink and B. Reif, *J. Am. Chem. Soc.*, 2009, **131**, 14018–14022.

14 P. Schanda, B. H. Meier and M. Ernst, *J. Am. Chem. Soc.*, 2010, **132**, 15957–15967.
15 P. Ma, J. D. Haller, J. Zajakala, P. Macek, A. C. Sivertsen, D. Willbold, J. Boisbouvier and P. Schanda, *Angew. Chem., Int. Ed.*, 2014, **53**, 4312–4317.
16 M. Weingarth, A. Prokofyev, E. A. van der Cruijsen, D. Nand, A. M. Bonvin, O. Pongs and M. Baldus, *J. Am. Chem. Soc.*, 2013, **135**, 3983–3988.
17 M. Weingarth, E. A. W. van der Cruijsen, J. Ostmeyer, S. Lievestro, B. Roux and M. Baldus, *J. Am. Chem. Soc.*, 2014, **136**, 2000–2007.
18 R. Linser, U. Fink and B. Reif, *J. Am. Chem. Soc.*, 2009, **131**, 13703–13708.
19 D. H. Zhou and C. M. Rienstra, *J. Magn. Reson.*, 2008, **192**, 167–172.
20 J. R. Lewandowski, J.-N. Dumez, U. Akbey, S. Lange, L. Emsley and H. Oschkinat, *J. Phys. Chem. Lett.*, 2011, **2**, 2205–2211.
21 R. Linser, B. Bardiaux, S. G. Hyberts, A. H. Kwan, V. K. Morris, M. Sunde and G. Wagner, *J. Am. Chem. Soc.*, 2014, **136**, 11002–11010.
22 V. Agarwal, S. Penzel, K. Szekely, R. Cadalbert, E. Testori, A. Oss, J. Past, A. Samoson, M. Ernst, A. Böckmann and B. H. Meier, *Angew. Chem., Int. Ed.*, 2014, **53**, 12253–12256.
23 D. H. Zhou, G. Shah, M. Cormos, C. Mullen, D. Sandoz and C. M. Rienstra, *J. Am. Chem. Soc.*, 2007, **129**, 11791–11801.
24 D. H. Zhou, A. J. Nieuwkoop, D. A. Berthold, G. Comellas, L. J. Sperling, M. Tang, G. J. Shah, E. J. Brea, L. R. Lemkau and C. M. Rienstra, *J. Magn. Reson.*, 2012, **54**, 291–305.
25 E. Barbet-Massin, A. J. Pell, K. Jaudzems, W. T. Franks, J. S. Retel, S. Kotelovica, I. Akopjana, K. Tars, L. Emsley, H. Oschkinat, A. Lesage and G. Pintacuda, *J. Biomol. NMR*, 2013, **56**, 379–386.
26 A. Marchetti, S. Jehle, M. Felletti, M. J. Knight, Y. Wang, Z. Q. Xu, A. Y. Park, G. Otting, A. Lesage, L. Emsley, N. E. Dixon and G. Pintacuda, *Angew. Chem., Int. Ed.*, 2012, **51**, 10756–10759.
27 S. Penzel, A. A. Smith, V. Agarwal, A. Hunkeler, A. Samoson, A. Böckmann, M. Ernst and B. H. Meier, *J. Biomol. NMR*, 2015, **63**, 165–186.
28 J. M. Lamley, D. Iuga, C. Öster, H.-J. Sass, M. Rogowski, A. Oss, J. Past, A. Reinhold, S. Grzesiek, A. Samoson and J. R. Lewandowski, *J. Am. Chem. Soc.*, 2014, **136**, 16800–16806.
29 D. H. Zhou, J. J. Shea, A. J. Nieuwkoop, W. T. Franks, B. J. Wylie, C. Mullen, D. Sandoz and C. M. Rienstra, *Angew. Chem., Int. Ed.*, 2007, **46**, 8380–8383.
30 S. Xiang, V. Chevelkov, S. Becker and A. Lange, *J. Biomol. NMR*, 2014, **60**, 85–90.
31 S. Xiang, K. Grohe, P. Rovó, S. Vasa, K. Giller, S. Becker and R. Linser, *J. Biomol. NMR*, 2015, **62**, 303–311.
32 L. B. Andreas, J. Stanek, T. Le Marchand, A. Bertarello, D. Cala-De Paepe, D. Lalli, M. Krejčíková, C. Doyen, C. Öster, B. Knott, S. Wegner, F. Engelke, I. C. Felli, R. Pierattelli, N. E. Dixon, L. Emsley, T. Herrmann and G. Pintacuda, *J. Biomol. NMR*, 2015, **62**, 253–261.
33 M. von Bergen, P. Friedhoff, J. Biernat, J. Heberle, E. M. Mandelkow and E. Mandelkow, *Proc. Natl. Acad. Sci. U. S. A.*, 2000, **97**, 5129–5134.
34 V. Chevelkov, B. Habenstein, A. Loquet, K. Giller, S. Becker and A. Lange, *J. Magn. Reson.*, 2014, **242**, 180–188.
35 N. Gustke, B. Trinczek, J. Biernat, E.-M. Mandelkow and E. Mandelkow, *Biochemistry*, 1994, **33**, 9511–9522.
36 O. C. Andronesi, M. von Bergen, J. Biernat, K. Seidel, C. Griesinger, E. Mandelkow and M. Baldus, *J. Am. Chem. Soc.*, 2008, **130**, 5922–5928.
37 V. Daebel, S. Chinnathambi, J. Biernat, M. Schwalbe, B. Habenstein, A. Loquet, E. Akoury, K. Tepper, H. Müller, M. Baldus, C. Griesinger, M. Zweckstetter, E. Mandelkow, V. Vijayan and A. Lange, *J. Am. Chem. Soc.*, 2012, **134**, 13982–13989.